Available online at www.sciencedirect.com
ScienceDirect
Sedimentary Geology 198 (2007) 221–232
Sedimentary Geology
www.elsevier.com/locate/sedgeo

"Cherty" stringers in the Barnett Shale are agglutinated foraminifera

Kitty Milliken [a,*], Suk-Joo Choh [b], Petro Papazis [c], Jürgen Schieber [d]

[a] Department of Geological Sciences, Jackson School of Geosciences, University of Texas at Austin, Austin, TX 78712, United States
[b] Department of Earth and Environmental Sciences, Korea University, Anam-Dong, Seongbuk-Gu, Seoul 136-713, Republic of Korea
[c] Chevron International E & P Co. 1500 Louisiana St., Room 29072B Houston, TX 77002, United States
[d] Department of Geological Sciences, Indiana University, 1001 E 10th Str., Bloomington, Indiana 47405, United States

Received 11 July 2006; accepted 13 December 2006

Abstract

Masses of microcrystalline quartz are abundant within several lithologies in the Barnett Shale (lower Mississippian) of central Texas. A typical quartz mass is elongated parallel to bedding and contains a central planar microporous structure that suggests collapse of a formerly hollow spheroidal or tubular body. An integrated imaging approach, utilizing transmitted polarized light microscopy, secondary and back-scattered electron imaging, cathodoluminescence imaging, and X-ray mapping reveals these quartz masses to be composed primarily of quartz-cemented silt-size detrital quartz with a minor admixture of detrital Ca-plagioclase and dolomite.

Microcrystalline quartz-rich masses in the Barnett Shale are interpreted as agglutinated foraminifera that have been dramatically collapsed during compaction. Locally, a significant portion of the total detrital quartz resides within these biogenic accumulations. This study highlights the potential for using these imaging techniques to investigate agglutinated foraminifera in lithified materials that are not amenable to disaggregation and extraction of three-dimensional specimens. The combined imaging techniques provide an unambiguous view into aspects of skeletal ultrastructure, such as particle size and sorting, that cannot be readily obtained from either conventional light microscopy or SEM. These techniques reveal that agglutinated foraminifers are abundant in several lithologies of the Barnett Shale, pointing to the possibility that application in other organic-rich shales may reveal these organisms to be more widespread than previously recognized. Comparative observations in Devonian shales of the central eastern United States support this prediction.

Keywords: Agglutinated foraminifera; Black shale; Barnett Shale; Quartz diagenesis; Cathodoluminescence

1. Introduction

We report here significant local accumulations of quartz (stringers) in a Paleozoic black siliceous shale (lower Mississippian Barnett Shale, Fort Worth Basin) that are interpreted as the collapsed tests of agglutinated foraminifera (Papazis et al., 2005). In transmitted polarized light microscopy these masses appear convincingly authigenic (chert-like) and without further information these could be easily interpreted as silicified examples of collapsed spores or algal cysts such as *Tasmanites*. Confirmation of the mixed detrital and

* Corresponding author. Tel.: +1 512 471 6082; fax: +1 512 471 9425.
E-mail address: kittym@mail.utexas.edu (K. Milliken).

0037-0738/$ - see front matter © 2006 Elsevier B.V. All rights reserved.
doi:10.1016/j.sedgeo.2006.12.012

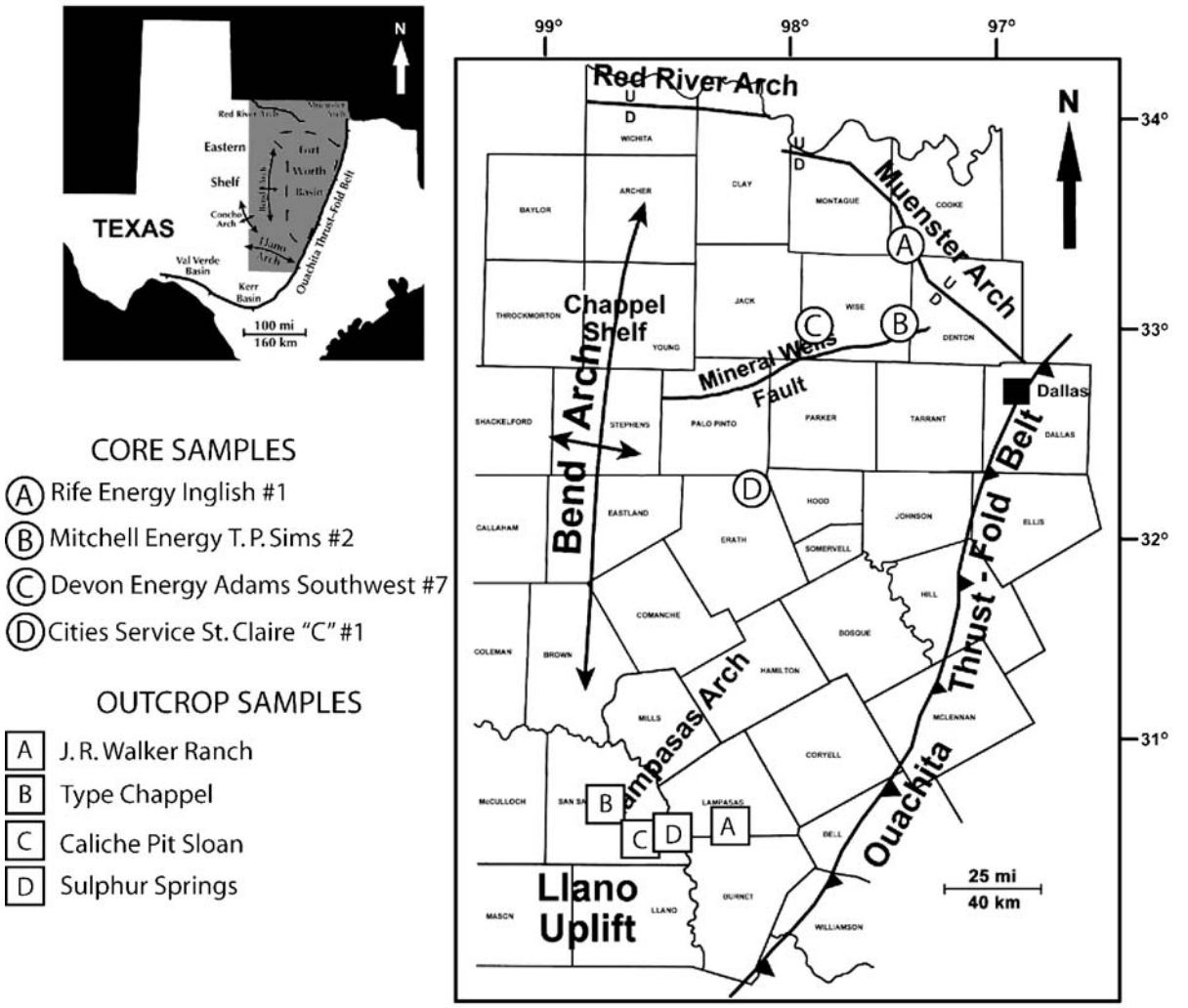

Fig. 1. Location map showing outcrops and cores of the Barnett Shale utilized in this study (modified from Montgomery et al., 2005; Papazis, 2005).

authigenic nature of the quartz requires use of back-scattered electron imaging and SEM-based cathodoluminescence. This technical approach has implications for understanding the distribution, composition, and ultrastructure of agglutinated foraminifera, the balance between authigenic and detrital silica in shales, and for interpreting the environmental conditions of black shale deposition.

2. Barnett Shale of central Texas

The Early Mississippian Barnett Shale is an important gas-producing unit in the Fort Worth Basin of north-central Texas (Montgomery et al., 2005) (Fig. 1). This basin is bounded on the east by the Ouachita fold and thrust belt, on the west by the Bend Arch, on the south by the Precambrian crystalline Llano Uplift, and on the north by the Muenster and Red River Arches. The basin formed as a Late Paleozoic foreland associated with the advancing Ouachita Front (Arbenz, 1989).

The Barnett Shale contains diverse lithologies but can be described broadly as a classic Paleozoic siliceous black shale (Papazis, 2005). The unit is dominated by silty shale and clayey micrite with local accumulations of silty biomicrite, fossiliferous silty shale, and fossiliferous intraclast conglomerate containing abundant phosphate clasts. Some of the coarser grained layers contain skeletal components derived from a diverse assemblage of marine invertebrates including brachiopods, sponges, pelecypods, gastropods,

cephalopods, conodonts, and echinoderms. Locally, calcite-cemented zones within carbonate-rich lithologies take the form of concretions.

3. Sampling, sample preparation, and imaging methods

Barnett Shale samples were obtained from outcrop and core (Fig. 1). Seventy seven samples representing the major lithologic variations were thin sectioned. Thin section blanks were cut perpendicular to bedding and the polished thin sections were prepared following vacuum-pressure impregnation. A few sections cut parallel to bedding were also prepared for comparison. Textural preservation during the final polish was enhanced by repeated surface application of a low-viscosity impregnation medium during progressive polishing.

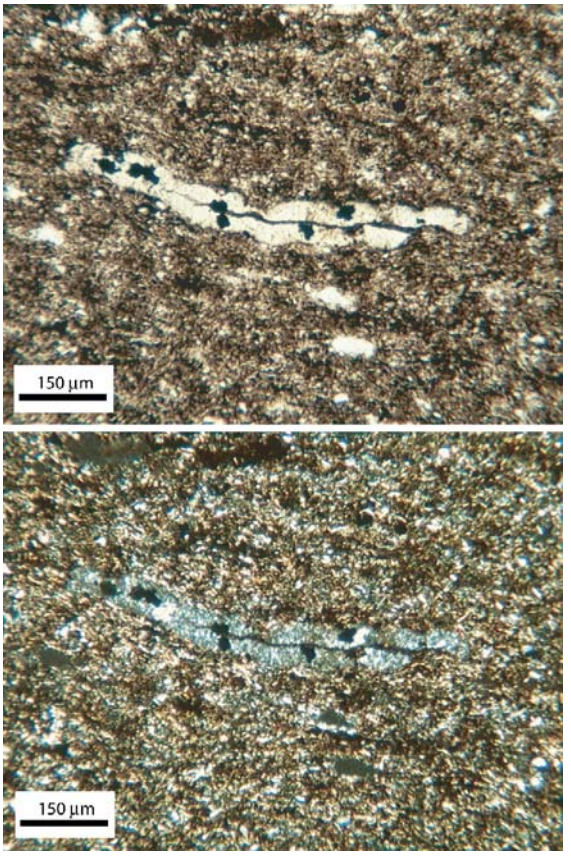

Fig. 2. Typical 'cherty stringer' in silty black shale. Sample PXK-25, depth=4988 ft, Cities Service St. Clair "C" No. 1, Erath County, Texas. A. Plane-polarized light. Black inclusions are authigenic pyrite. B. Cross-polarized light. Bright inclusions are carbonate, possibly detrital.

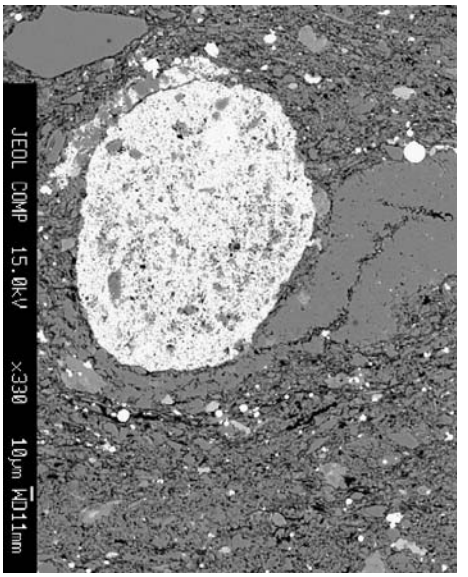

Fig. 3. Compactional compression of a microcrystalline quartz mass around a phosphate intraclast (p); detrital silt particle (s, upper right) is accompanied by many similar small particles. Back-scattered electron image. Sample PXK-4, Mitchell Energy T. P. Sims #2, Wise County, Texas.

All of the thin sections were examined using conventional transmitted polarized light microscopy. Selected samples were carbon-coated and examined using back-scattered electron (BSE) imaging on a JEOL 8200 electron microprobe (15 KV accelerating voltage, sample current in the range of 12–15 nA). Spot analyses (beam has approximately 1 µm diameter) for qualitative elemental composition were performed by energy dispersive spectroscopy X-ray analysis (EDS). X-ray mapping (stage mapping) for Si, Mg, K, Na, and Fe was performed by wavelength dispersive spectrometry (WDS) using a 15 KV accelerating voltage, a 25 nA sample current, a 40 ms dwell time, and a 1 µm pixel size. Scanned cathodoluminescence (CL) imaging was performed in conjunction with secondary electron (SE) imaging on a Philips/FEI XL 30 ESEM using an accelerating voltage of 12 KV and a sample current near 90% of maximum. The CL signal was collected with a Gatan PanaCL-2 equipped with RGB filters.

For comparison, additional CL and charge-contrast images from Barnett Shale samples and from Devonian shales (Schieber, 2005) were obtained using a FEI Quanta 400 FEG (field emission SEM) located in the Department of Geological Sciences at Indiana University, Bloomington (IUB). The IUB SEM is equipped with a Gatan Chroma CL color cathodoluminescence detector that can scan CL images up to 16 megapixels in

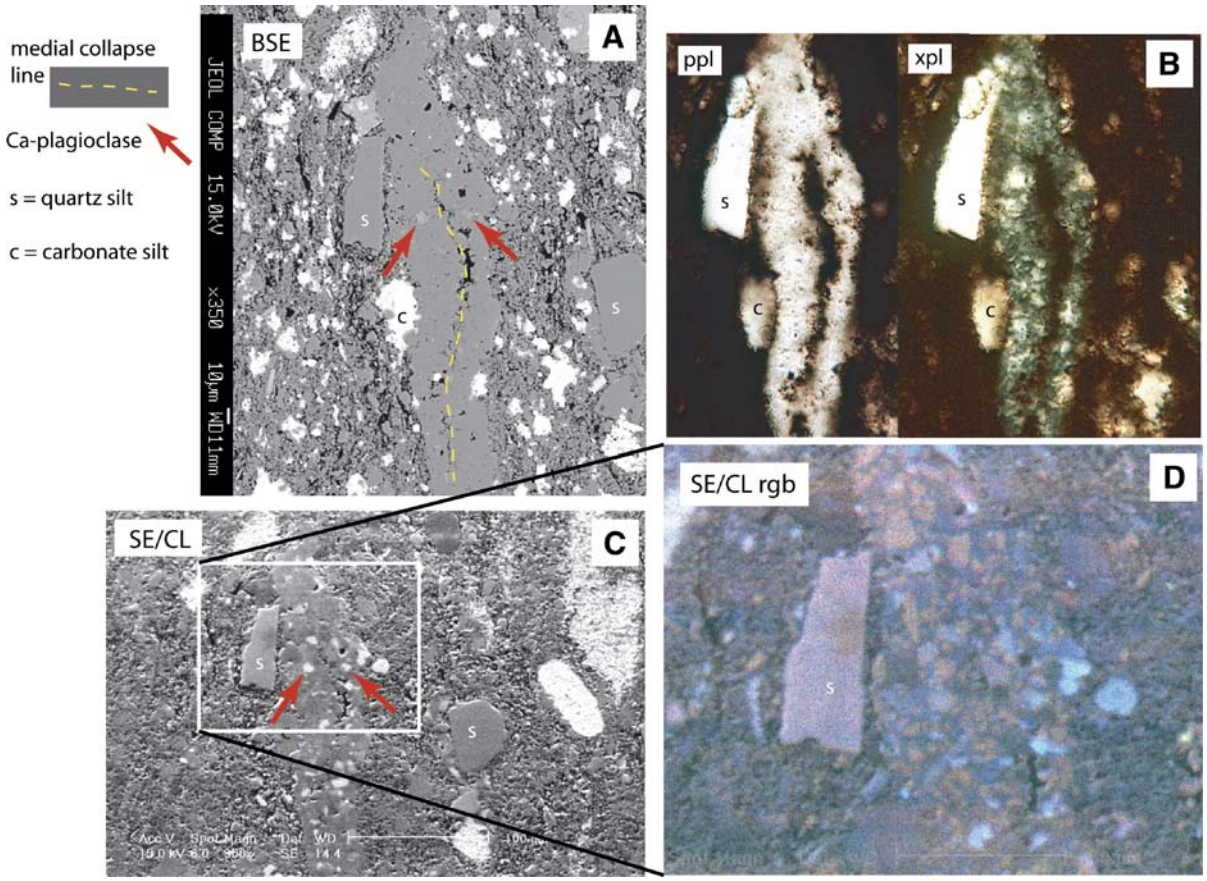

Fig. 4. A single microcrystalline quartz mass seen in five different imaging modes. In each image, bedding is aligned vertically. An angular silt particle (s) to the left of the microcrystalline quartz mass provides a useful marker for comparing the images. Mineralogies indicated below were determined by EDS. Sample PXK-3, Mitchell Energy T. P. Sims #2, Wise County, Texas. A. Back-scattered electron image. Red arrows indicate small Ca-plagioclase crystals of angular shape. A calcitic particle (c) is seen on the left side. Pores are black. Yellow line marks the microporous dark structure seen in images in B. B. Plane-polarized (left) and cross-polarized (right) transmitted light images. Here the dark medial line, the small non-quartz inclusions, and the microcrystalline nature of the quartz are apparent. C. Panchromatic CL/SE image. Here the variable CL intensity of the various microcrystals can be appreciated. Note that the Ca-plagioclase grains are very bright, as is typical of high-temperature feldspars. D. RGB CL image. Here the variable colors of the microcrystals are apparent.

size, and can resolve micron-size and smaller quartz grains. Charge-contrast imaging was done in a low-vacuum mode at chamber pressures between 90 and 120 Pa.

4. Imaging data

4.1. Quartz in the Barnett Shale

Quartz in Barnett shale samples occurs in several forms. Among crystals large enough to be observed petrographically, volumetrically significant forms of quartz include angular monocrystals, elongate microcrystalline quartz masses, replacements of calcareous skeletal debris, and small vein fills (Papazis, 2005; Papazis and Milliken, 2005). The angular monocrystals are clearly extrabasinal detritus, based upon their shape (Milliken, 1994), variable CL color and intensity, lack of zoning, and diverse mineral and fluid inclusions including apatite, zircon, and rutile (Papazis, 2005; Papazis and Milliken, 2005). The following petrographic description focuses on the elongate microcrystalline quartz masses, although the petrographic character of the angular monocrystals (labeled "s") can also be examined in many of the accompanying photomicrographs.

4.2. General form of microcrystalline quartz masses

Typical elongate microcrystalline quartz masses are within the range of 50 to 100 μm thick with aspect ratios

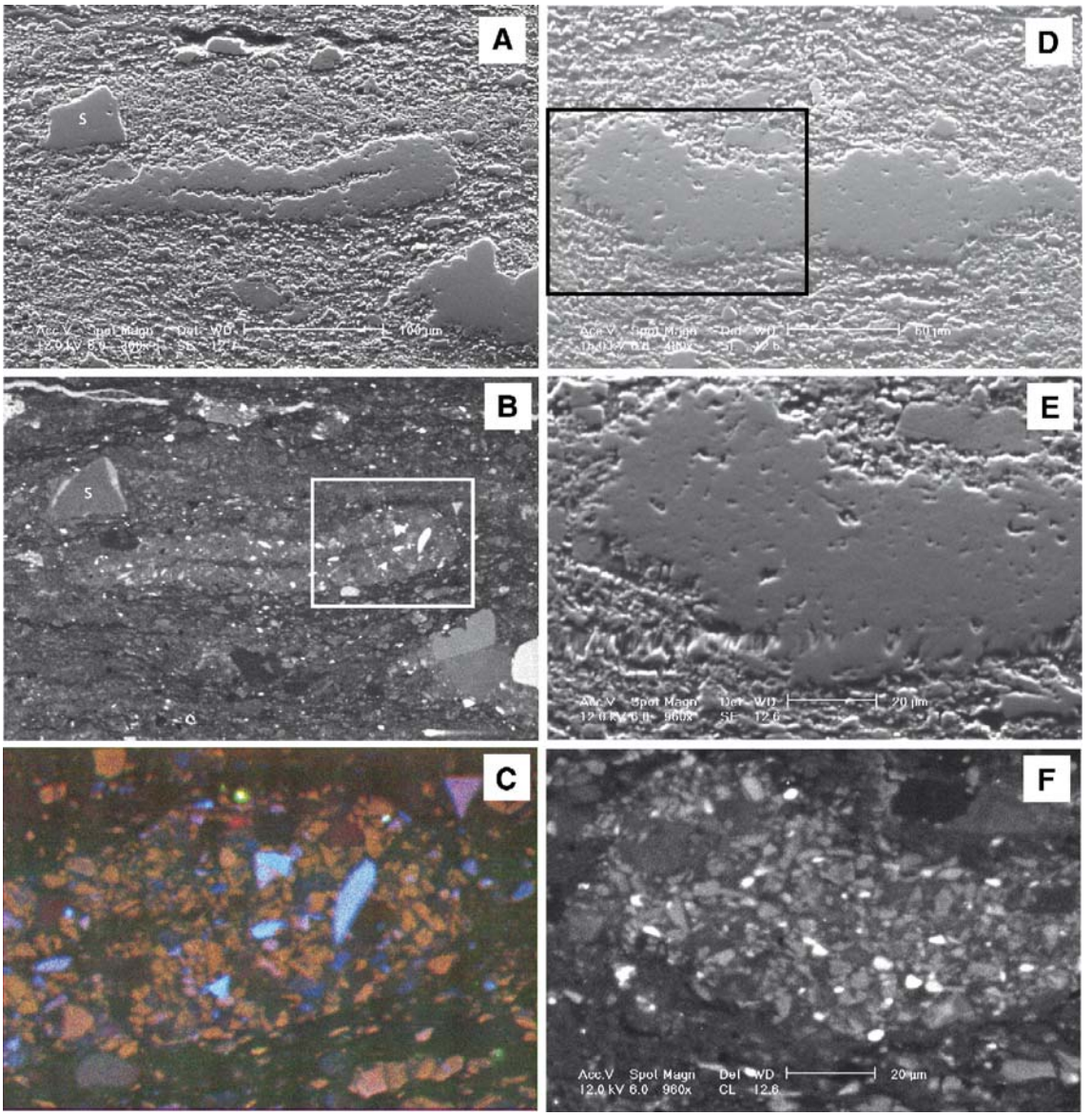

Fig. 5. Additional examples of microcrystalline quartz masses. A. Secondary electron image. Small quartz mass with a prominent central porous zone stands out in relief because of its greater resistance during polishing. Sample PXK-4, Mitchell Energy T. P. Sims #2, Wise County, Texas. B. Panchromatic CL image of the region depicted by image 5A. C. RGB CL image of the area indicated by the white box in image 5B. CL intensity and color variations and angular shapes are apparent amongst the microcrystals. D. Secondary electron image. Quartz mass lacking a medial microporous zone. Sample PXK-4, Mitchell Energy T. P. Sims #2, Wise County, Texas. E. Secondary electron image of the area indicated by the black box in image 5D. F. Panchromatic CL of the same field of view seen in 5E. CL intensity variations and angular shapes are apparent amongst the microcrystals.

in the range of 10:1 (length:thickness) (Fig. 2). These masses are aligned parallel to bedding. Many, though not all, contain a central crudely planar structure that is dark in plane light (described in more detail below) and typically extends to within 25 to 50 µm of the ends of the mass. Some of the masses are prominently deformed by differential compaction around more rigid particles (typically phosphatic intraclasts), leading in some cases to a somewhat wavy or crenulate appearance to the overall mass (Fig. 3).

4.3. Petrographic character of quartz in microcrystalline quartz masses

Cross-polar observation reveals the microcrystalline nature of the elongate quartz masses (Figs. 2B, 4B).

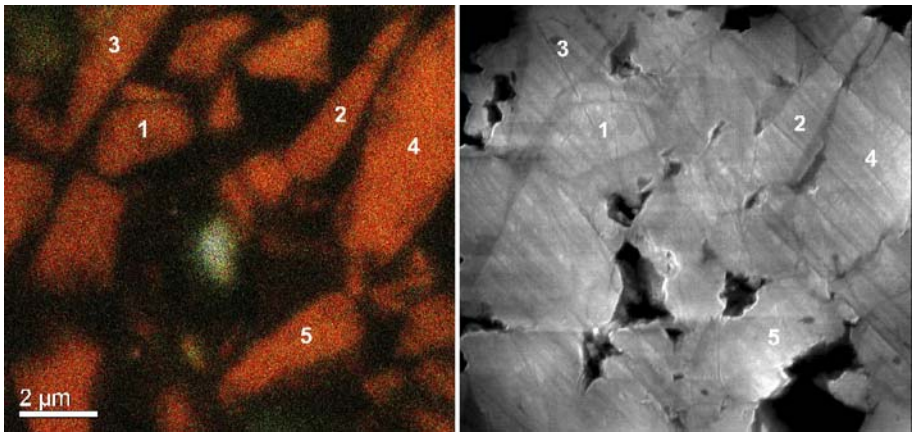

Fig. 6. Contrasting quartz types within the microcrystalline quartz masses that are visible in CL (left) are also apparent in charge-contrast images (right). Numbers indicate detrital grains that are correlative between the two images. Sample PXK-4, Mitchell Energy T. P. Sims #2, Wise County, Texas.

Crystals range in size from 1 to 10 μm and have no obvious preferred orientation.

CL imaging reveals that the individual microcrystals vary widely in CL intensity (below detection to very bright; Figs. 4C, 5B,F) and CL color (shades ranging from blue to reddish-orange; Figs. 4D, 5C). This same range of CL properties is seen in the quartz monocrystals (detrital silt) that are scattered throughout the shale (Fig. 4C, D).

In CL imaging, individual quartz microcrystals are revealed to consist of relatively bright-luminescing cores surrounded by dark-luminescing quartz (Figs. 4C D, 5C F). The relatively bright-luminescing portions of the

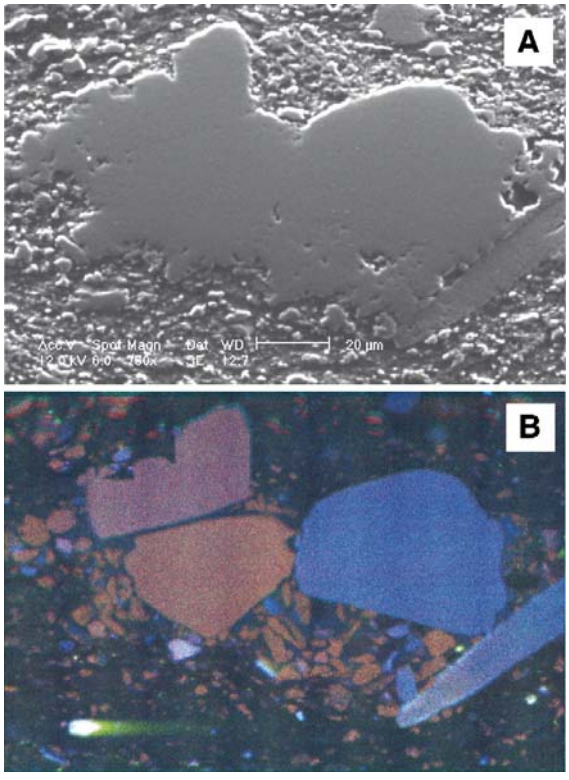

Fig. 7. Quartz mass that contains both sand-size and silt-size crystals. Sample PXK-4, Mitchell Energy T. P. Sims #2, Wise County, Texas. A. SE image. B. RGB CL image. Elongate, blue-luminescing particle on the right side is an echinoderm spine.

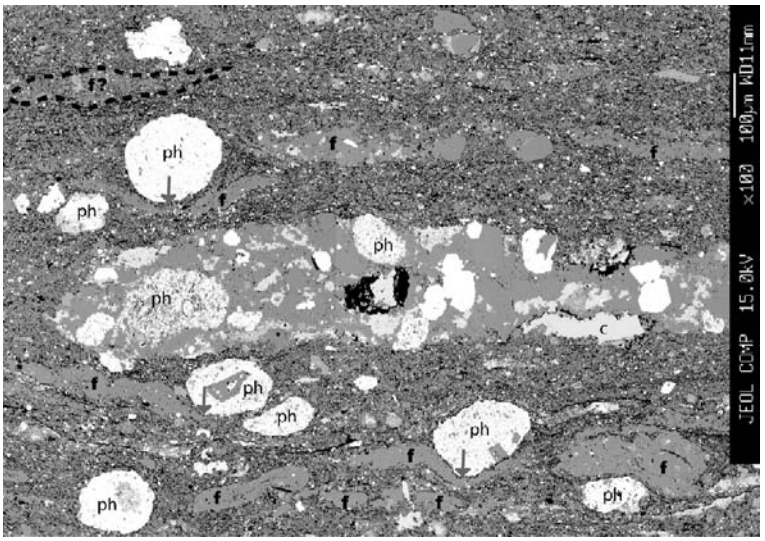

Fig. 8. Large, sand-bearing quartz mass with a significant admixture of non-quartz components including phosphatic intraclasts (ph) and carbonate particles (c). Bright euhedra are authigenic pyrites that have replaced quartz. Additional microcrystalline quartz masses are seen scattered through the image (f). Locally, the quartz masses are deformed (arrows) around phosphate clasts (ph). Back-scattered electron image. Sample PXK-4, Mitchell Energy T. P. Sims #2, Wise County, Texas.

microcrystals have angular shapes. The bright-luminescing versus dark-luminescing portions of the microquartz can also be discriminated in charge-contrast images (Fig. 6). Although most microquartz masses are composed exclusively of crystals smaller than 10 μm, some masses contain an admixture of sand-size quartz crystals (Fig. 7). Sand-bearing masses tend to be larger overall, reaching thicknesses of 300 μm and tend to contain a particle assemblage of more diverse mineralogy (e.g., phosphatic intraclasts, skeletal fragments, etc.; Fig. 8).

4.4. Non-quartz components in microcrystalline quartz masses

BSE images of the microcrystalline masses, together with EDS and X-ray mapping, reveal a minor component of Ca-plagioclase crystals that have sizes and angular shapes similar to those of the angular quartz microcrystals (Fig. 4A). The CL intensity of Ca-plagioclase crystals is relatively bright (Fig. 4C).

In plane light the elongate microcrystalline quartz masses also contain minute ($\leq$1–5 μm) pores and brownish inclusions scattered through the quartz (Fig. 2). BSE and SE imaging confirms that the overall region of microcrystalline quartz is microporous and that the central planar structure to be especially so (Figs. 4A,B, 5A,D, 8A). In plane light the central planar structure contains dark material with color and texture similar to that of the surrounding clay-rich sediment. X-ray mapping confirms that this central dark region contains K that is common to the surrounding mica- and clay-rich matrix, but is otherwise absent within the quartz-rich portion of the mass (Fig. 9B).

5. Distribution of microcrystalline quartz-rich masses in the Barnett Shale

Out of 77 thin sections examined, at least 60% of the samples contain the elongate microcrystalline quartz-rich masses described above. Microcrystalline quartz-rich masses are observed in all of the major lithologies, with the exceptions of the concretions, but they are most abundant, perhaps not surprisingly, in the silty black shales. Locally, within silty black shales, these masses incorporate a significant portion of all the detrital silt (Fig. 9A,C). There is a somewhat negative correlation between the occurrence of microcrystalline quartz masses and the amount of carbonate, either as micrite or skeletal debris, present in the rock. Microcrystalline quartz masses do however occur in some of the phosphate-rich intraclastic layers (Fig. 10).

6. Observations in other black shales

In an effort to determine the broader applicability of the findings reported here for the Barnett Shale, additional observations have been made on Devonian shales of the eastern US (Schieber, 2005). Black shales that range in age from Givetian to Famennian (Lazar and Schieber, 2004) were examined in the Illinois Basin

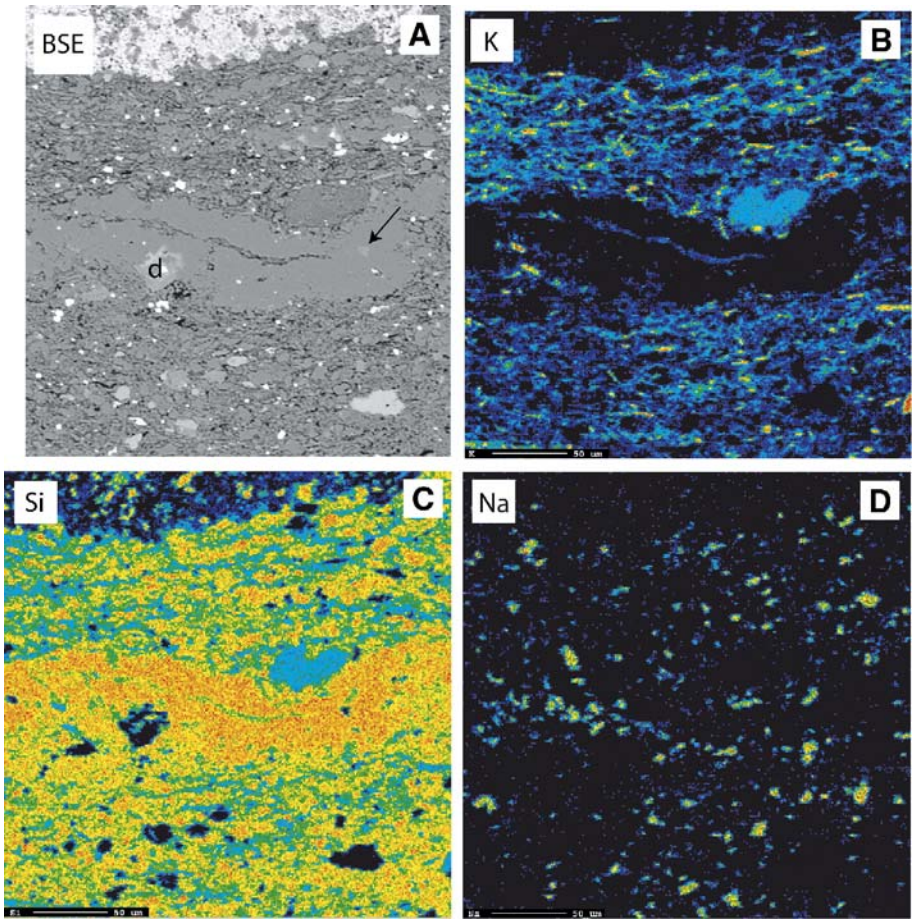

Fig. 9. A single microcrystalline quartz mass seen in four imaging modes that highlight the non-quartz components and mineralogical selectivity displayed by these aggregates. In each image, bedding is aligned horizontally. Sample PXK-4, Sample PXK-4, Mitchell Energy T. P. Sims #2, Wise County, Texas. A. Back-scattered electron image. Arrow indicates an angular dolomite crystal (identified by EDS); another, larger, dolomite is labeled (d). Possibly detrital dolomite crystals are common in the Barnett. B. K-map. Reds correspond to the highest K-concentrations. Elongate red/yellow crystals are micas. Note the absence of micas within the microcrystalline quartz mass. The microporous medial zone contains K similar in concentration to regions of the image corresponding to the matrix clays. C. Si-map. Highest Si (orange) corresponds to quartz. A significant amount of the total quartz in this field of view is concentrated within the microcrystalline quartz mass. D. Na-map. Highest Na-concentrations correspond to detrital feldspars (mostly albite, but including Ca-plagioclase) that are widely distributed both in the matrix and the microcrystalline mass.

(New Albany Shale) and in the Appalachian Basin (Ohio Shale). Lenticular bodies of fine-crystalline silica that are of the same appearance as those described from the Barnett Shale are found in many shale samples that were examined petrographically (Fig. 11). Color cathodoluminescence and charge-contrast imaging of these chert-like bodies show them to consist of silica-cemented detrital quartz grains and confirms that they are similar to the features we have described here for the Barnett.

7. Discussion

The bulk of the quartz and feldspar within the microcrystalline quartz masses of the Barnett Shale is interpreted as detrital particles (silt and some sand) on the basis of their shapes (very angular) and the variable intensity, color, and texture of their cathodoluminescence. Cathodoluminescence variability is a hallmark of detrital quartz (e.g., Zinkernagel, 1978; Owen, 1991), including detrital quartz silt (Milliken, 1994). This conclusion is supported by the similar ranges of CL intensity and color observed for isolated detrital particles that are scattered through the shale. Dark-luminescing quartz (Sippel, 1968) between the angular-shaped detrital particles is interpreted as authigenic quartz cement. The fact that charge-contrast images also render these distinct quartz types within the microcrystalline masses visible further supports the interpretation that these quartz forms carry contrasting

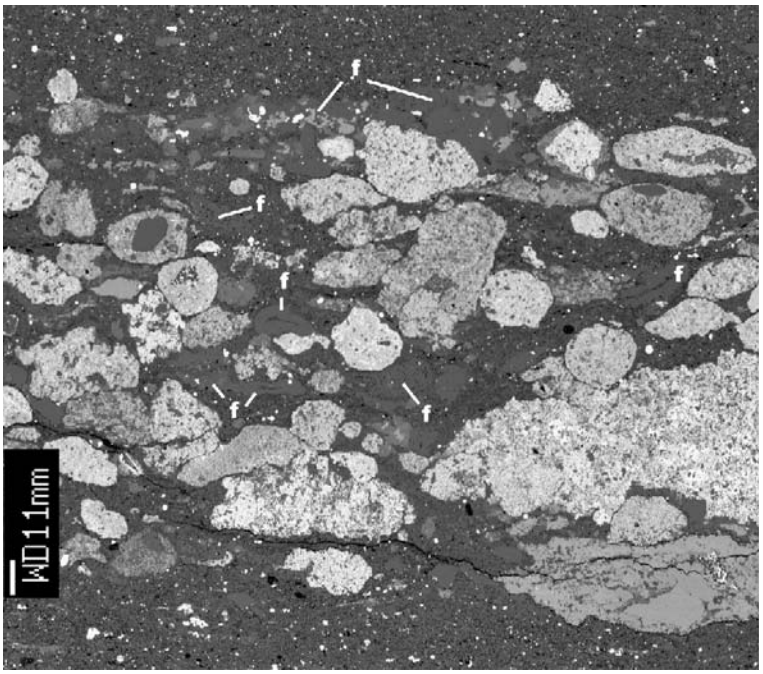

Fig. 10. Diverse microcrystalline quartz aggregates (f) within a phosphatic intraclast layer. Sample PXK-4, Mitchell Energy T. P. Sims #2, Wise County, Texas.

defect populations and, thus, have distinctly different origins.

The rare feldspar crystals included within the microcrystalline quartz masses are likewise interpreted as detrital. This is based on their angular shapes and bright CL intensity, as well as their composition, as authigenic Ca-plagioclase is not reported to form diagenetically.

The near-total exclusion of the abundant detrital micas and clays from the quartz-rich microcrystalline masses is difficult to explain on the basis of mechanical sorting processes. An interpretation as silt-rich burrow fills is ruled out because extremely well-sorted silt layers that could supply such material to the burrows are not observed in the cores. Compacted spores or algal cysts such as *Tasmanites* have sizes and shapes similar to the quartz-rich microcrystalline masses (e.g., Combaz, 1980; Stach and Murchison, 1982), but the presence of a substantial detrital quartz component in the walls rules out authigenic silicification of these fossils as an explanation.

The favored interpretation, of course, is that these elongate microcrystalline quartz-rich masses are the highly compacted tests of agglutinated foraminifera. This is supported by the character of the detrital grain assemblage (quartz plus feldspar, excluding micas), the overall shape of the masses, and the medial microporous and clay-bearing features that are interpreted to be formed by compactional collapse of the test chamber(s).

Agglutination is the earliest form of foraminiferal test construction (e.g., Ross and Ross, 1991; McIlroy et al., 2001; Scott et al., 2003), and many Paleozoic agglutinated foraminifera have single-chambered forms (e.g., Ross and Ross, 1991; Flügel, 2004). It is well-established that agglutinated foraminifers in modern environments are highly tolerant of conditions of low-oxygenation (e.g., Bernhard, 1989; Bernhard and Reimers, 1991; SenGupta and Machain-Castillo, 1993; Gooday, 1994), and occur in various marine environments from brackish coastal water to marine abyssal environments (e.g., Chekhovskaya, 1973; Haunold et al., 1997; Hughes, 1988; Flügel, 2004). Agglutinated foraminifera have been previously identified in mudrocks and black shales (e.g., Gutschick and Wuellner, 1983; Gebhardt, 1997; Holbourn et al., 2001), largely based on observations of three-dimensional specimens prepared using acid treatment and disaggregation.

The microporous nature of agglutinated tests and the occurrence of authigenic quartz as a cementing agent within some species has been previously documented using secondary electron imaging (e.g., Jorgensen, 1977; Mendelson, 1982; Weston, 1984; Bender and Hemleben, 1988; Mancin, 2001). Our imaging results

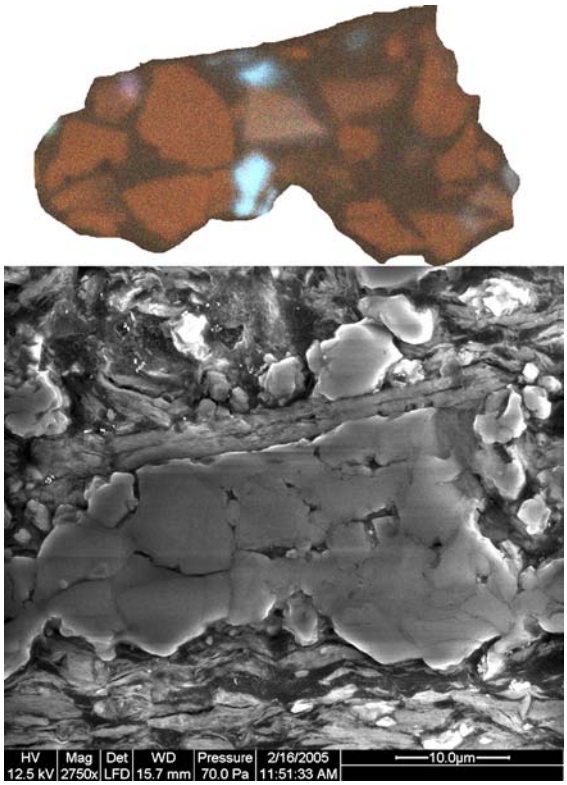

Fig. 11. Microcrystalline quartz mass seen in secondary electron image (bottom) and RGB CL (top). Devonian, New Albany Shale.

confirm the presence of microporosity and authigenic quartz although we are unable to determine if the authigenic quartz replaces a precursor opaline cementing agent or an organic matrix.

Despite the potential benefits with respect to understanding wall structure (Jorgensen, 1977) as well as species diversity and lithologic associations of foraminiferal assemblages (Reolid and Herrero, 2004), thin sections have not been widely applied in the study of agglutinated foraminifers. In the case of the Barnett, the extreme compaction of the agglutinated masses poses significant challenge to the study of three-dimensional specimens, as does the highly lithified character of Barnett lithologies. Based on the variations observed for wall thickness, aspect ratio, grain size distribution, grain population compositions, and lithologic distribution we speculate that diverse taxa are found within the Barnett. Given the ease and frequency with which agglutinated foraminifers can be located within all the black shales we have examined to date, we further speculate that agglutinated foraminifers are more abundant and widely distributed in black shales than what is generally recognized. With the aid of the back-scattered electron- and CL imaging described here, a more detailed assessment of agglutinate diversity and distribution in black shales is in progress.

Previous work has documented that quartz in shales can take several forms including extrabasinal detritus (e.g., Blatt and Schultz, 1976; Blatt, 1987; Milliken, 1994), microcrystalline replacements of opaline skeletal debris or volcanic ash, vein fills (Papazis and Milliken, 2005), and authigenic pore fills (Schieber, 1996; Land and Milliken, 2000). This study reveals that detrital and authigenic modes of occurrence can, in fact, be intimately linked at the microscale by the agency of agglutinated foraminifera.

8. Conclusions

Microcrystalline quartz masses in the Barnett Shale are the remains of collapsed agglutinated foraminifera. Various lines of petrographic evidence from CL, BSE, and X-ray mapping support a detrital origin for silt-size fragments of quartz and feldspar within the masses. Together with the overall form and size of the masses and the presence of medial collapse sutures, the detrital nature of the aggregates supports an origin as the walls of agglutinated foraminifera. Silica cementation within

the aggregates suggests (but may not prove) that the original walls were partially biomineralized by opal. Compactional collapse of the foraminiferal tests has dramatically altered their shapes. Agglutinated foraminifers effectively aggregated much of the detrital quartz within some Barnett lithologies and created distinctive quartz masses that could easily be mistaken for authigenic quartz in the absence of CL or BSE imaging. It is critical that microcrystalline quartz-rich masses in black shales be examined with scanned-CL before they are interpreted as authigenic. The abundance and widespread distribution of agglutinated foraminifera in the Barnett Shale suggests that workers should be alert to the presence of these fossils in other siliceous black shales.

Acknowledgments

This study was supported by the Geology Foundation of the Jackson School of Geosciences, The University of Texas at Austin. We thank Michael Cameron of Devon Corporation for providing access to core samples. Work on Devonian black shales by JS is supported by the Petroleum Research Fund (ACS PRF #38523-AC8), and by an NSF equipment grant (EAR-0318769) for acquisition of an analytical SEM. Discussions with Joe Macquaker, Robert Folk, and Earle McBride supported our efforts to interpret petrographic observations in Barnett Shale.

References

Arbenz, J.K., 1989. The Ouachita system. In: Bally, A.W., Palmer, A.R. (Eds.), The Geology of North America—An Overview. The Geology of North America. Geological Society of America, Boulder, Colorado, pp. 371–396.

Bender, H., Hemleben, C., 1988. Constructional aspects in test formation of some agglutinated foraminifera. In: Rogl, F., Gradstein, F.M. (Eds.), Second Workshop on Agglutinated Foraminifera. Abhandlungen der Geologischen Bundesanstalt, Vienna, pp. 13–21.

Bernhard, J.M., 1989. The distribution of benthic foraminifera with respect to oxygen concentration and organic carbon levels in shallow-water Antarctic sediments. Limnology and Oceanography 34, 1131–1141.

Bernhard, J.M., Reimers, C.E., 1991. Benthic foraminiferal population fluctuations related to anoxia: Santa Barbara Basin. Biogeochemistry 15, 127–149.

Blatt, H., 1987. Oxygen isotopes and the origin of quartz. Journal of Sedimentary Petrology 57, 373–377.

Blatt, H., Schultz, D.J., 1976. Size distribution of quartz in mudrocks. Sedimentology 23, 857–866.

Chekhovskaya, M.P., 1973. Distribution of benthic foraminifers in the northeastern Bering Sea. Oceanology 13, 571–575.

Combaz, A., 1980. Les kerogenes vus au microscope. In: Durand, B. (Ed.), Kerogen. Technip, Paris, pp. 55–111.

Flügel, E., 2004. Microfacies of Carbonate Rocks. Springer, Berlin (976 pp).

Gebhardt, H., 1997. Cenomanian to Turonian foraminifera from Ashaka (NE Nigeria): quantitative analysis and palaeoenvironmental interpretation. Cretaceous Research 18, 17–36.

Gooday, A.J., 1994. The biology of deep-sea foraminifera: a review of some advances and their applications in paleoceanography. Palaios 9, 14–31.

Gutschick, R.C., Wuellner, D., 1983. An unusual benthic agglutinated foraminiferan from Late Devonian anoxic basinal black shales of Ohio. Journal of Paleontology 57, 308–320.

Haunold, T.G., Baal, C., Piller, W.E., 1997. Benthic foraminiferal associations in the NOrthern Bay of Safaga, Red Sea, Egypt. Marine Micropaleontology 29, 185–210.

Holbourn, A., Kuhnt, W., Erbacher, J., 2001. Benthic foraminifers from lower Albian black shales (Site 1049, ODP Leg 171): evidence for a non "uniformitarian" record. Journal of Foraminiferal Research 31, 60–74.

Hughes, G.W., 1988. Modern bathyal agglutinating foraminifera from the Vella Gulf and Blanche Channel, New Georgia, Solomon Islands, southwest Pacific. Journal of Foraminiferal Research 18, 304–310.

Jorgensen, N.O., 1977. Wall structure of some arenaceous foraminfera from the Maastrichtian white chalk (Denmark). Journal of Foraminiferal Research 7, 313–321.

Land, L.S., Milliken, K.L., 2000. Regional loss of SiO_2 and $CaCO_3$ and gain of K_2O during burial diagenesis of Gulf Coast mudrocks, USA. In: Worden, R.H., Morad, S. (Eds.), Quartz Cementation in Sandstones. Special Publication. International Association of Sedimentologists, pp. 183–198.

Lazar, O.R., Schieber, J., 2004. New Albany and Ohio Shales: an introduction. In: Schieber, J., Lazar, O.R. (Eds.), Devonian Black Shales of the Eastern U.S.: New Insights into Sedimentology and Stratigraphy from the Subsurface and Outcrops in the Illinois and Appalachian Basins. Field Guide for the 2004 Great Lakes Section SEPM Annual Field Conference. Open File Study. Indiana Geological Survey, pp. 31–34.

Mancin, N., 2001. Agglutinated foraminifera from the Epiligurian succession (middle Eocene/lower Miocene, northern Apennines, Italy): scanning electron microscopic characterization and paleoenvironmental implications. Journal of Foraminiferal Research 31, 294–308.

McIlroy, D., Green, O.R., Brasier, M.D., 2001. Palaeobiology and evolution of the earliest agglutinated foraminifera: playsolenites, sipirsolenites, and related forms. Lethaia 34, 13–29.

Mendelson, C.V., 1982. Surface texture and wall structure of some recent species of agglutinated foraminifera (Textulariina). Journal of Paleontology 56, 295–307.

Milliken, K.L., 1994. Cathodoluminescent textures and the origin of quartz silt in Oligocene mudrocks, South Texas. Journal of Sedimentary Research 64A, 567–571.

Montgomery, S.L., Jarvie, D.M., Bowker, K.A., Pollastro, R.M., 2005. Mississippian Barnett Shale, Fort Worth Basin, north-central Texas: gas-shale play with multi-trillion cubic foot potential. American Association of Petroleum Geologists Bulletin 89, 155–175.

Owen, M.R., 1991. Application of cathodoluminescence to sandstone provenance. In: Barker, C.E., Kopp, O.C. (Eds.), Luminescence Microscopy and Spectroscopy: Quantitative and Qualitative Applications. SEPM, pp. 67–75.

Papazis, P.K., 2005. Petrographic characterization of the Barnett Shale, Fort Worth Basin, Texas. M. S. Thesis, University of Texas at Austin, Austin, Texas.

Papazis, P.K., Milliken, K.L., 2005. Cathodoluminescent textures and the origin of quartz in the Mississippian Barnett Shale, Fort Worth Basin, Texas, Annual Meeting. American Association of Petroleum Geologists, Calgary, Alberta, p. A105.

Papazis, P.K., Milliken, K.L., Choh, S.-J., Schieber, J., Maquaker, J., 2005. The Widespread Occurrence of Agglutinated Foraminifera in Black Shales, Annual Meeting. Geological Society of America, Salt Lake City Utah.

Reolid, M., Herrero, C., 2004. Evaluation of methods for retrieving foraminifera from indurated carbonates: application to the Jurassic spongiolithic limestone lithofacies of the Prebetic Zone (South Spain). Micropaleontology 50, 307–312.

Ross, C.A., Ross, J.R.P., 1991. Paleozoic foraminifera. BioSystems 25, 39–51.

Schieber, J., 1996. Early diagenetic silica deposition in algal cysts and spores: a source of sand in black shales? Journal of Sedimentary Research 66, 175–183.

Schieber, J., 2005. Agglutinated Foraminifera in Devonian Black Shales of the Eastern U.S.: Implications for Paleoenvironmental Reconstructions, Geological Society of America Abstracts with Program. Geological Society of America.

Scott, D.B., Medioli, F., Braund, R., 2003. Foraminifera from the Cambrian of Nova Scotia: the oldest multichambered foraminifera. Micropaleontology 49, 109–126.

SenGupta, B.K., Machain-Castillo, M.L., 1993. Benthic foraminifera in oxygen-poor habitats. Marine Micropaleontology 20, 183–201.

Sippel, R.F., 1968. Sandstone petrology, evidence from luminescence petrography. Journal of Sedimentary Petrology 38, 530–554.

Stach, E., Murchison, D., 1982. Stach's Textbook of Coal Petrology. Gebruder Borntraeger, Berlin. (535 pp.).

Weston, J.F., 1984. Wall structure of the agglutinated foraminifera *Eggerella bradyi* (Cushman) and *Karreriella bradyi* (Cushman). Journal of Micropalaeontology 3, 29–31.

Zinkernagel, U., 1978. Cathodoluminescence of quartz and its application to sandstone petrology. Contributions to Sedimentology, vol. 8. E. Schweizerbart'sche Verlagsbuchandlung (Nägele und Obermiller), Stuttgart (69 pp.).